Electrochimica Acta 167 (2015) 97–104

Contents lists available at ScienceDirect

Electrochimica Acta

journal homepage: www.elsevier.com/locate/electacta

Synthesis, characterization and electrochemical performances of nanocrystalline $FeVO_4$ as negative and $LiCoPO_4$ as positive electrode for asymmetric supercapacitor

V.D. Nithya [a], K. Pandi [a], Y.S. Lee [b], R. Kalai Selvan [a,*]

[a] Solid State Ionics and Energy Devices Laboratory, Department of Physics, Bharathiar University, Coimbatore-641 046, India
[b] Faculty of Applied Chemical Engineering, Chonnam National University, Gwangju 500-757, South Korea

ARTICLE INFO

Article history:
Received 26 January 2015
Received in revised form 2 March 2015
Accepted 14 March 2015
Available online 17 March 2015

Keywords:
Iron vanadate
Aqueous electrolyte
Olivine lithium cobalt phosphate
Asymmetric Supercapacitor

ABSTRACT

Iron vanadate, $FeVO_4$ nanoparticles are synthesized by simple co-precipitation method and explored as the pseudocapacitor negative electrode for the first time. The structural analysis shows the highly crystalline nature and phase purity of the material. The morphological features of $FeVO_4$ particles are polyhedral in shape and are in the range of 100–200 nm. The well defined lattice fringes corroborate the highly crystalline nature of $FeVO_4$. The $FeVO_4$ electrode exhibits a pronounced supercapacitive performance in 1 M KOH electrolyte than 1 M NaOH and 1 M LiOH electrolytes due to its smaller hydration sphere radii, increased mobility and ionic conductivity. The obtained higher specific capacitance of 972 F g^{-1} at 2 mV s^{-1} and 922 F g^{-1} at 2 mA cm^{-2}, inferred that it could be utilized as a suitable negative electrode. On the other hand, $LiCoPO_4$ is tested as the positive electrode (0 to 0.5 V) for the first time and delivers a specific capacitance of 320 F g^{-1} at 5 mV s^{-1}. Finally, an asymmetric supercapacitor is fabricated using $FeVO_4$ as negative and $LiCoPO_4$ as positive electrodes. The device exhibits an excellent energy density of 21 Wh kg^{-1} with a power density of 1326 W kg^{-1} in the potential range between 0 to 1.6 V.

1. Introduction

Supercapacitors are considered as one of the newest advances in the field of energy storage and conversion devices due to its attractive features such as high power density, long cycle life, etc. [1]. Generally, supercapacitors are classified into two types including (i) Electric double layer capacitor (EDLC) and (ii) Pseudocapacitor [2]. In EDLC's, the carbon based materials are used as the electrodes, where the charges are accumulated at the electrode–electrolyte interface [3,4]. In pseudocapacitors, the conducting polymers and metal oxides are employed as electrodes and the redox reactions are the reason for charge storage mechanism [5,6]. The energy density (E) of the supercapacitor is calculated by $E = CV^2/2$, where C is the specific capacitance and V is the operating cell voltage. According to this relation, the energy density (E) is proportional to the specific capacitance (C) and square of the operating voltage (V) of the supercapacitor. Hence, the effective way of improving the energy density is to enhance the specific capacitance of the materials and widening the operating potential window of the supercapacitor.

There are numerous reports on the positive electrode materials with high capacitances working in a wide potential window [7–12]. The existing positive electrode material, RuO_2 provides high specific capacitance of 1580 F g^{-1} [7] however, its high cost and toxicity limits the wide utility. Therefore, variety of metal oxides including NiO (690 F g^{-1} at 0.1 A g^{-1} in the potential of −0.3 V to +0.35 V), $NiCo_2O_4$ (1588 F g^{-1} at 1 A g^{-1} in the potential of 0 to +0.7 V), MnO_2 (411.9 F g^{-1} at 0.25 A g^{-1} in the potential of -0.2 V to +0.8 V), Co_3O_4 (456 F g^{-1} at 1 A g^{-1} in the potential of −0.1 V to +0.5 V), Mn_3O_4 (232.5 F g^{-1} at 0.5 A g^{-1} in the potential of 0 to +1.0 V) and CuO (212 F g^{-1} at 0.41 mA mg^{-1} in the potential of 0 to +0.4 V) has been revealed as the less expensive positive electrodes [5,8–12].

Therefore, identification of suitable negative electrode is an imperative one to counter balance the charges and to obtain the superior supercapacitive performance. There are some reports on the negative electrodes for supercapacitors such as Fe_3O_4, Fe_2O_3, Bi_2O_3, VN, etc. [13–16]. However, the obtained specific capacitance of these materials is insufficient for practical applications. The obtained capacitance is 163 F g^{-1} at 1 A g^{-1} for Fe_3O_4-carbon nanosheets in the potential range between −0.2 and −0.8 V [13]. Sethuraman et al. has utilised Fe_2O_3/C nanocomposites as the

* Corresponding author.
E-mail address: selvankram@buc.edu.in (R. K. Selvan).

http://dx.doi.org/10.1016/j.electacta.2015.03.107
0013-4686/

negative electrode and reported a specific capacitance of 315 F g^{-1} in 2 M KOH (+0.2 to −0.7 V) at 2 mV s^{-1} [14]. Similarly, Bi_2O_3 provided the specific capacitance of 250 F g^{-1} at 100 mV s^{-1} in 1 M Na_2SO_4 electrolyte (−0.2 to −1.0 V) [15] and vanadium nitride (VN) delivered a specific capacitance of 413 F g^{-1} at 1 A g^{-1} in the potential range of 0 to −1.1 V [16]. Although the capacitance rendered by the negative electrodes is quite enough, they are further insufficient to match the higher capacitances of the positive electrodes such as NiO (1085 F g^{-1}), $Ni(OH)_2$–$Co(OH)_2$ (2684 F g^{-1}), $Ni_3V_2O_8$ (1284 F g^{-1}), etc [17–19].

In this line, the present work concentrated on the synthesis of $FeVO_4$ nanoparticles by simple co-precipitation method. The iron based oxide *i.e.* $FeVO_4$ is chosen as the electrode material for supercapacitor since the availability of multiple oxidation states of iron, possess high potential window in aqueous solution upto −1.2 V, low cost, natural abundances and non-toxicity [20]. Normally, $FeVO_4$ has four different polymorphs named as $FeVO_4$-I, $FeVO_4$-II, $FeVO_4$-III, and $FeVO_4$-IV, whereas $FeVO_4$-I has the stable phase formed at room temperature and the rest of them are metastable phase that are usually formed at high pressure and high temperature. It is reported that the $FeVO_4$ has unique applications in various fields, including electrodes for Li-ion batteries, photocatalyst, gas sensors, etc. [21–23]. Thorough investigations on the structural, electrical and magnetic properties of $FeVO_4$ have been reported by us previously [24,25]. Consequently, in this present work an ample analysis of electrochemical performance of $FeVO_4$ is reported in various aqueous electrolytes such as 1 M LiOH, 1 M NaOH and 1 M KOH for the suitability of the negative electrodes. Normally, the supercapacitive performance of the electrodes is largely dependent on the hydration sphere radii, mobility and ionic conductivity of the electrolyte ions and hence it is essential to optimize the suitable electrolyte [26,27]. Subsequently, an asymmetric supercapacitor is fabricated using $FeVO_4$ as negative and new $LiCoPO_4$ as the positive electrode and studied their performances. Also in the present work, $LiCoPO_4$ is utilized as positive electrode for the first time.

2. Experimental Methods and Materials

2.1. Synthesis of $FeVO_4$

For the typical synthesis of $FeVO_4$ (3 g), the stoichiometric amount of Fe $(NO_3)_3.9H_2O$ (*i.e.* 7.096 g), NH_4VO_3 (2.052 g), NaOH (0.702 g) was dissolved in double distilled water individually. The dissolved aqueous Fe $(NO_3)_3{\cdot}9H_2O$ was added into Triton X-100 (10 ml) in 100 ml of distilled water under magnetic stirring. Then

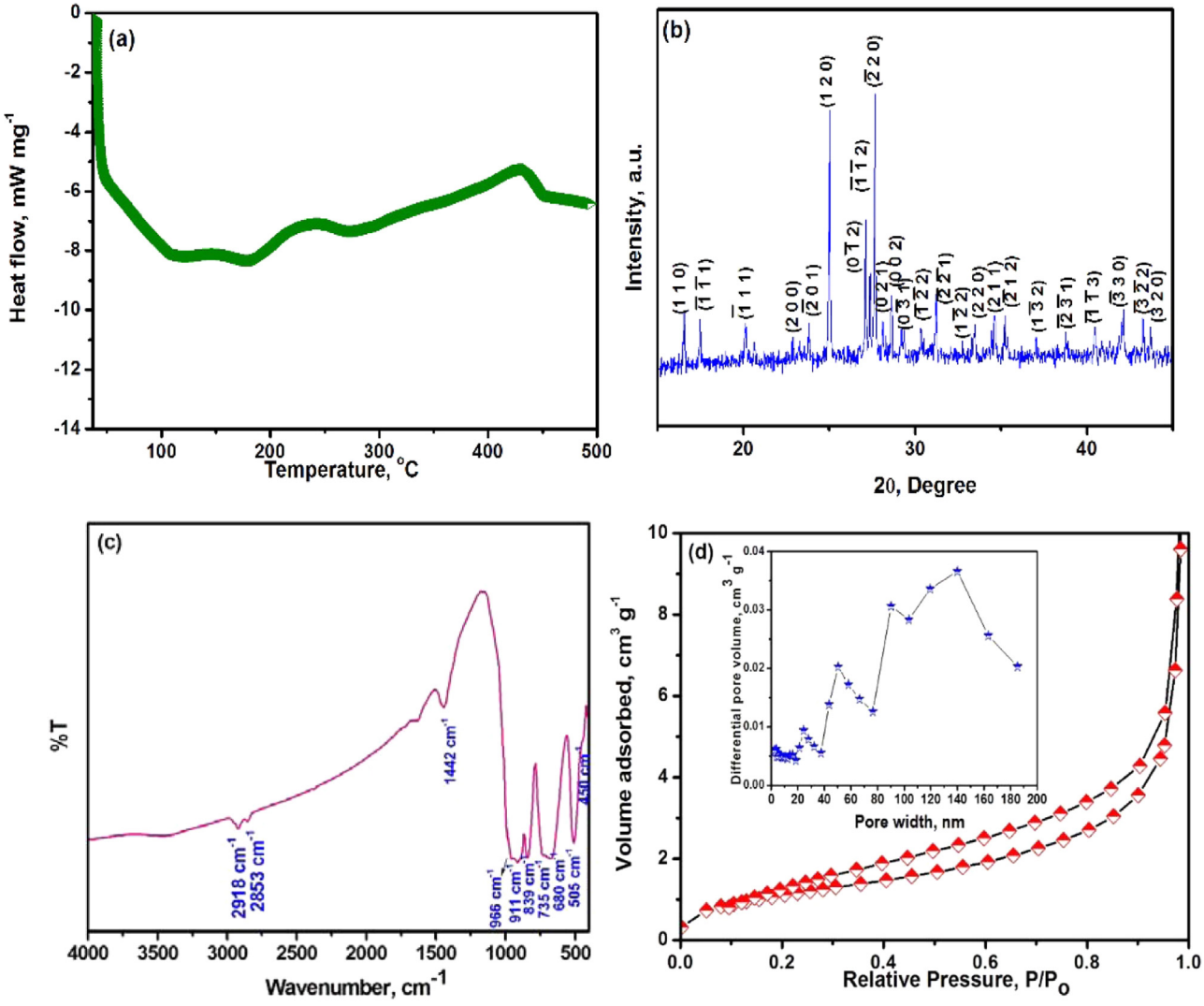

Fig. 1. (a) DSC curve (b) XRD pattern (c) FTIR spectrum (d) N_2 adsorption–desorption isotherms (Inset: Pore size distribution curve) of $FeVO_4$.

NH_4VO_3 was added, followed by NaOH solution. The pH of the solution was found to be 2. The above solution was stirred for another half an hour and kept undisturbed for 24 h. The obtained precipitate was washed several times with double distilled water and ethanol to remove impurities and dried overnight at 100 °C. Finally, the material was calcinated at 600 °C for 3 h.

2.2. Synthesis of $LiCoPO_4$

The detailed experimental procedure and the characterization techniques of $LiCoPO_4$ are already given in our previous article [28]. Solution combustion synthesis method was adopted for the preparation of $LiCoPO_4$. Briefly, the stoichiometric quantities of the starting materials such as Lithium chloride (LiCl), Cobalt nitrate ($Co(NO_3)_2{\cdot}6H_2O$) and Ammonium dihydrogen phosphate ($NH_4H_2PO_4$) were taken and dissolved in double distilled water individually and mixed together with the addition of urea [$(NH_2)_2CO$] as a fuel (pH 10). Subsequently, the mixed solution was heated at 100 °C to get a sticky paste and ignited the combustion reaction at about 400 °C to form a foamy powder. Finally, the obtained foamy powder was calcinated at 800 °C for 5 h to improve the crystallinity.

2.3. Characterization techniques:

The as prepared $FeVO_4$ material dried at 100 °C was subjected to Differential Scanning Calorimetry (DSC) analysis that was performed in air atmosphere using DSC Q20V24. The material calcined at 600 °C was characterized by various techniques such as XRD (X-Ray Diffraction), Fourier Transform Infrared Spectroscopy (FT-IR), FE-SEM (Field Emission Scanning Electron Microscope) and HR-TEM (High Resolution Transmission Electron Microscope) analysis respectively. XRD was carried out using BRUKER D8 Advance with CuKα radiation, FT-IR through SHIMADZU Model IR Affinity 1, FESEM and HRTEM using Quanta FEG 250 and JEOL JEM 2100 respectively. In addition, Nitrogen adsorption desorption measurements were performed using Micromeritics ASAP 2010 surface area analyzer. The electrochemical performance was investigated using cyclic voltammetry (CV), Galvanostatic charge–discharge (GCD) and electrochemical impedance spectroscopy (EIS).

The electrochemical measurements were carried out in a three electrode system containing an active material coated onto the graphite material as the working electrode, graphite as the counter electrode and Hg/HgO as reference electrode respectively. The active material, carbon black and PVDF are taken in the weight ratio of 80:15:5 which is made into slurry by adding NMP (0.3 ml). Then 8 μl of slurry is then coated onto a graphite electrode ($1 \times 1\ cm^2$) and dried at 60 °C for the whole night. The mass of the active material coated is 1 mg. The cyclic voltammetry, charge–discharge, electrochemical impedance analysis was carried out using the SP-150 BIO-LOGIC science workstation. The electrochemical impedance spectrum was studied in the frequency range between 10 mHz–1 MHz.

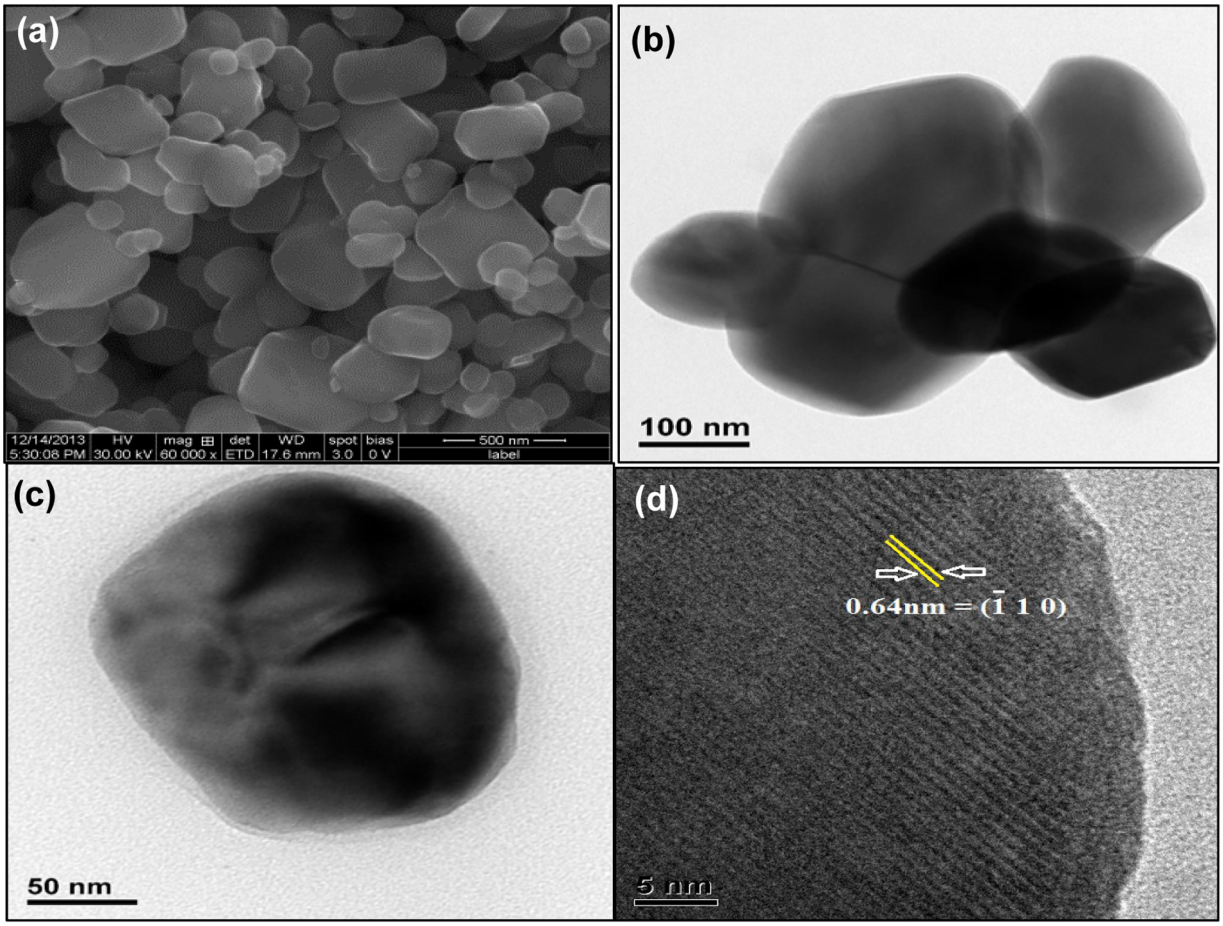

Fig. 2. (a) FE-SEM (b & c) TEM (d) HRTEM image of $FeVO_4$.

3. Results and discussion

3.1. Structural and electrochemical analysis of $FeVO_4$

The thermal behavior of the prepared material is characterized by DSC analysis. The DSC curve of $FeVO_4$ is shown in Fig. 1(a). It can be seen that there is a wide endothermic peak observed in between 100–250 °C, followed by a sharp exothermic peak between 390–450 °C. The wide endothermic peak observed in between 100–250 °C corresponds to the dehydration of adsorbed water molecules in the $FeVO_4$ [29]. The observed sharp exothermic peak between 390–450 °C may be due to the transformation from the amorphous phase into the crystalline $FeVO_4$ triclinic structure or a temperature of crystallization [30,31]. It is also reported that, this exothermic peak is the characteristic peak of the oxidation of organic residues present in the material [32]. It is also noted from the figure that, there is a slight endothermic peak observed in the range of 250–300 °C which is due to the removal of coordinated water within the crystal structure [33].

The XRD pattern of the 600 °C calcinated $FeVO_4$ is given in Fig. 1(b). It shows the sharp and well defined peaks indicating the high crystalline nature of the material. The obtained diffraction pattern is well matched with the standard (JCPDS. 38-1372) and possess triclinic structure. The calculated lattice parameters are a = 8.0518 Å, b = 9.3618 Å, c = 6.7120 Å, α = 106.65°, The obtained diffraction pattern β = 101.38° and γ = 96.76° which is in agreement with the standard values. The standard values are a = 8.0572 Å, b = 9.347 Å, c = 6.7138 Å, α = 106.590°, β = 101.526° and γ = 96.69°. Subsequently, the observed cell volume and lattice density are 466.92 $Å^3$ and 3.259 g cm^{-3}, respectively.

In order to further confirm the presence of possible functional groups in $FeVO_4$, FTIR analysis is carried out. The corresponding FTIR spectrum is shown in Fig. 1(c). It can be seen that the bands observed at 1050–850 cm^{-1} corresponds to the stretching of short vanadyl (V=O) bonds [34] and at 911 cm^{-1} attributes to V=O and V—O—V coupled vibrations [35]. Similarly, the band in the range of 830–700 cm^{-1} is due to the bridging V—O . . . ..Fe stretching [36,37]. As well as the broad peak at 700–500 cm^{-1} attributes to V—O . . . Fe and V-O..Fe mixed bridging stretching. The wave-number below 500 cm^{-1} attributes to the V—O—V deformations mixed with Fe—O stretching modes [36,37]. In addition to that, there is a presence of bands at 2853 and 2923 cm^{-1} which corresponds to CH_2 stretching vibrations [38]. The BET specific surface area of $FeVO_4$ is obtained using N_2 adsorption desorption experiments (Fig. 1(d)) The observed hysteresis type behavior infers that the materials having a slight porous nature and the calculated specific surface area is 4 $m^2 g^{-1}$. The average pore volume is 0.0227 $cm^3 g^{-1}$, which is calculated from the pore size distribution curve (Fig. 1(d) inset).

The morphological feature of $FeVO_4$ is analyzed using FE-SEM and TEM analysis. The FE-SEM image of $FeVO_4$ is shown in Fig. 2(a). As it is seen, the particles are found to be polyhedral in shape and randomly distributed. The average particle size (one side length) of the material is measured using the scion image software, and the maximum number of particles is found to be in the size range of 100–200 nm. Fig. 2(b–c) shows the TEM images of $FeVO_4$ in different magnifications. As it is seen from the figure, the shape of the particles is found to be polyhedral. The HRTEM image of $FeVO_4$ is shown in Fig. 2(d). The fringes are clearly visible and the d spacing values calculated from the fringes are in accordance with the XRD data. The d spacing value measured from the lattice fringe is found to be 0.64 nm that corresponds to $(\bar{1}10)$ lattice plane. The formation of $FeVO_4$ is also confirmed from HRTEM characterization.

The pseudocapacitive behavior of $FeVO_4$ is evaluated using electrochemical analysis, including cyclic voltammetry (CV), galvanostatic charge discharge (GCD) and EIS analysis is carried out using three electrode systems. The CV measurement of $FeVO_4$ is carried out in three different electrolytes such as 1 M LiOH, 1 M NaOH and 1 M KOH to optimize the suitable electrolyte. It is well known that the size and diffusion speed of the solvated electrolyte ions played a major role to determine the performance of the material. The CV curves of $FeVO_4$ in three different electrolytes such as 1 M LiOH, 1 M NaOH and 1 M KOH at 20 mV s^{-1} is shown in Fig. 3(a). A pair of redox peaks is clearly observed at −1.0 V and −0.5 V vs Hg/HgO.

The peak at −1.0 V is due to the reduction process given by [39],

$$Fe^{3+} + e^- \rightarrow Fe^{2+} \quad (1)$$

The oxidation reaction occurs at −0.5 V is given by,

$$Fe^{2+} \rightarrow Fe^{3+} + e^- \quad (2)$$

As it is seen from Fig. 3(a), the current area under CV curves is high in 1 M KOH electrolyte compared with 1 M NaOH and 1 M LiOH. It indicates that the $FeVO_4$ electrode possesses a higher value of capacitance in 1 M KOH. In general, the area under a CV curve is related to specific capacitance (C_{sp}) by the relation given by,

$$C_{sp} = \frac{\int IdV}{2.\Delta V.\Delta m.\nu} \quad (3)$$

Where ∫IdV is the integral area, ΔV is the potential window, Δm is the active material mass, ν is the scan rate.

A higher value of specific capacitance is observed in 1 M KOH, when compared with 1 M NaOH and 1 M LiOH. The values of

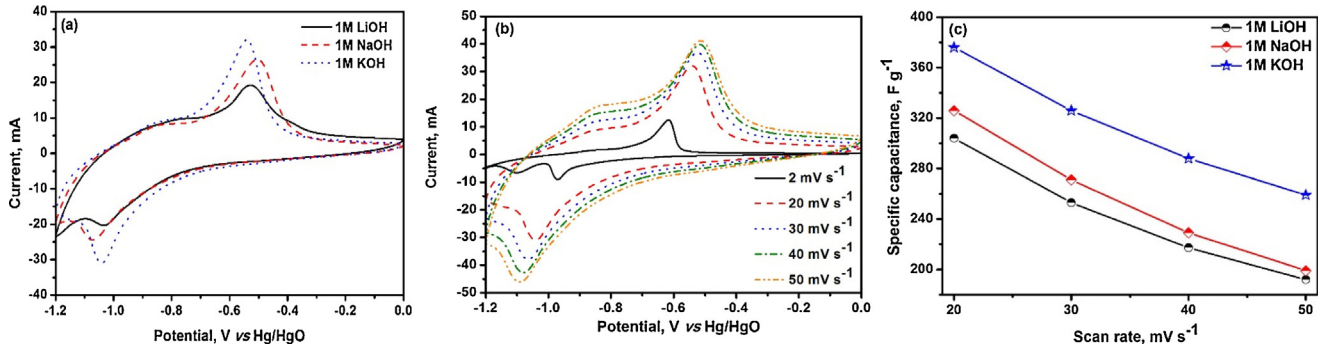

Fig. 3. (a) CV curves of $FeVO_4$ in various electrolytes at 20 mV/s^{-1} (b) CV curve in 1 M KOH electrolyte at different scan rates (c) Comparison of specific capacitance in various electrolytes at different scan rates.

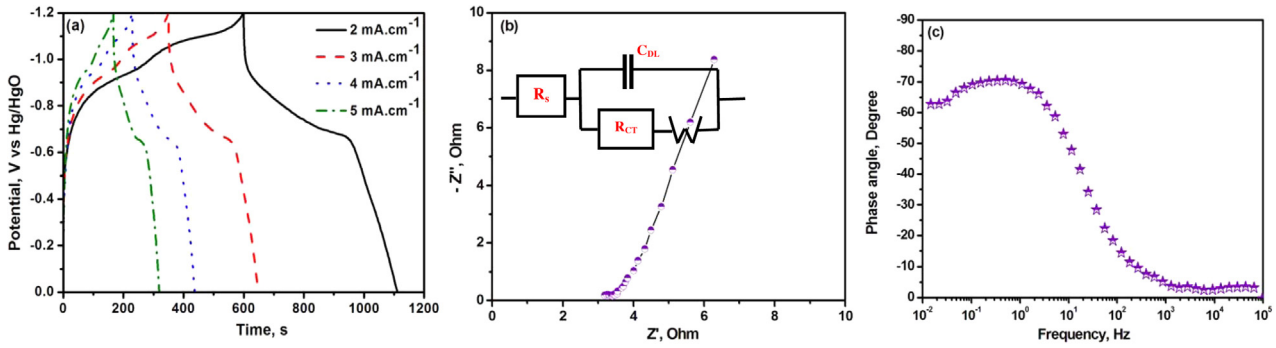

Fig. 4. (a) GCD curves of $FeVO_4$ at various current densities (b) EIS spectra (c) Phase angle *vs.* frequency plot in 1 M KOH electrolyte.

specific capacitance for 1 M LiOH, 1 M NaOH and 1 M KOH at 20 mV s^{-1} are 304, 326 and 376 F g^{-1} respectively. This variation arises due to the difference in hydrated radius of K^+ ions (3.31 Å), Na^+ ions (3.58 Å) and Li^+ ions (3.82 Å). Also, the reported ionic conductivity of K^+ ions (73 $cm^2\,\Omega^{-1}\,mol^{-1}$) is greater than Na^+ ions (50 $cm^2\,\Omega^{-1}\,mol^{-1}$) and Li^+ ions (38 $cm^2\,\Omega^{-1}\,mol^{-1}$) at 25 °C [40,41]. The lower hydrated radius of K^+ ions favors faster ionic mobility and interaction with the electrode material, thereby resulting in enhanced electrochemical performance.

The CV curves of $FeVO_4$ in the optimized KOH electrolyte at 2, 20, 30, 40 and 50 mV s^{-1} are given in Fig. 3(b). The obtained specific capacitances are 972, 376, 326, 288 and 259 F g^{-1} respectively. The specific capacitance is found to be higher at lower scan rates while it decreases upon increasing scan rates. The calculated specific capacitances in different electrolytes at various scan rates are given in Fig. 3(c). The obtained value of capacitance is very high compared to ν-Fe_2O_3 films, where a specific capacitance of 210 F g^{-1} is achieved at 2 mV s^{-1} in the potential range from −0.9 V to −0.1 V [42]. It is also higher than $VO_x{\cdot}nH_2O$ where a specific capacitance of 227.3 F g^{-1} is obtained at 200 mA g^{-1} in $NaNO_3$ solution [43].

The further electrochemical characterizations of $FeVO_4$ are carried out in the optimized 1 M KOH electrolyte. Fig. 4(a) shows the galvanostatic charge discharge (GCD) curves of $FeVO_4$ at different current densities in 1 M KOH electrolyte. It can be seen that a non-linear type of curves is observed that indicates the pseudocapacitive nature. It is well known, the larger discharge time would lead to higher specific capacitance [44]. The specific capacitances are calculated at various current densities [44], and they are 922, 824, 751 and 683 F g^{-1} for 2, 3, 4 and 5 mA cm^{-2} respectively.

The electrochemical conductive behavior of $FeVO_4$ is studied using electrochemical impedance spectral (EIS) analysis in the frequency range between 10 mHz and 1 MHz. The EIS spectrum of $FeVO_4$ is shown in Fig. 4(b). It can be seen that, there is a depressed semi-circle with a single vertical line observed at high frequency observed. The semi-circle in the mid-high frequency attributes to the charge transfer resistance (R_{CT}). Subsequently, the intersection of the impedance plot at the real axis in the high frequency region indicates the equivalent series resistance (R_s). The equivalent series resistance is a combination of ionic resistance of the electrolyte, the intrinsic resistance of the active material and the contact resistance at the active material/current collector interface [45,46]. The observed EIS spectra is fitted using the equivalent circuit consisting of Rs, R_{CT}, double layer capacitance (C_{DL}) and Warburg diffusion (W). The equivalent circuit is given as an inset of Fig. 4(b). The fitted parameters such as Rs, R_{CT}, C_{DL} and W are 3.15 Ω, 0.29 Ω, 3.8×10^{-3} F and 20.04 Ohm $s^{-1/2}$, respectively, where the Warburg diffusion is the frequency dependence of the ionic diffusion in the electrolyte [47]. The variation of phase angle as a function of frequency of $FeVO_4$ is given in Fig. 4(c). The phase angle is found to be −62° which clearly indicates the pseudocapacitive behavior of the material [48].

3.2. Structural and electrochemical analysis of $LiCoPO_4$ electrodes

The structural analysis of the prepared $LiCoPO_4$ is reported elsewhere [28]. Briefly, the X-ray diffraction analysis revealed the formation of phase purity and highly crystalline $LiCoPO_4$ with orthorhombic structure. The functional groups and vibrational

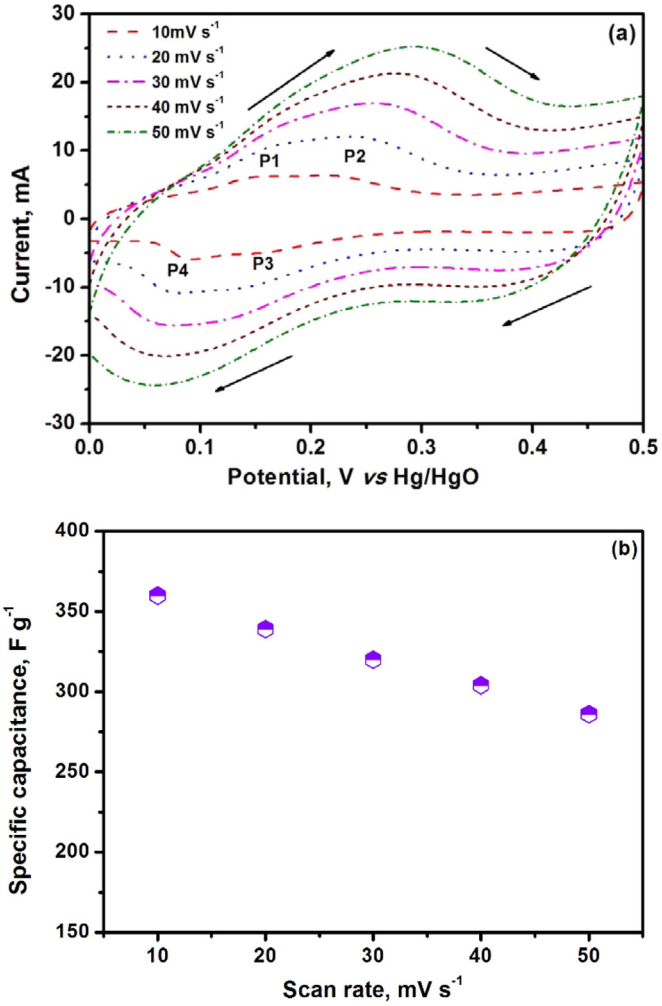

Fig. 5. (a) CV curves of $LiCoPO_4$ at various scan rates and (b) Scan rate vs specific capacitance.

modes of $LiCoPO_4$ were confirmed from FTIR and Raman analysis. X-ray photoelectron spectroscopy (XPS) analysis confirmed the presence of Co 2p, P 2p and O1s states in $LiCoPO_4$. The high-resolution scanning electron microscopic (HR-SEM) image showed the particles with irregular shape and their size ranged between 1–2 μm.

Herein, $LiCoPO_4$ is tested as pseudocapacitor electrode for the first time and its electrochemical performance is studied using cyclic voltammetric (CV) analysis. The $LiCoPO_4$ electrode exhibits the redox characteristics in the positive potential region from 0 to +0.5 V in 1 M KOH electrolyte. The CV curves of $LiCoPO_4$ at various scan rates are given in Fig. 5(a). There are two oxidation and reduction reaction are observed, where the occurred oxidation (P1) and reduction peak (P4) at lower potentials corresponds to the reversible reaction between Co (II) and Co(III) [49,50] and is given by Eq. (4),

$$Co^{2+} \leftrightarrow Co^{3+} + e^- \quad (4)$$

Also, the presence of oxidation (P2)/reduction (P3) peaks attributes to Co(III)/Co(IV) reversible reaction [49,50] and is given by Eq. (5),

$$Co^{3+} \leftrightarrow Co^{4+} + e^- \quad (5)$$

The specific capacitance at each scan rate is calculated and is given in Fig. 5(b). The calculated specific capacitance is 360, 339, 320, 304 and 286 F g^{-1} for 10, 20, 30, 40 and 50 mV s^{-1} respectively. The observed specific capacitance of $LiCoPO_4$ is higher than the reported positive electrodes such as V_2O_5, SnO_2, Mn_2O_3 etc. [51–53]. In brief, Bonso et al., has reported the synthesis of V_2O_5 nanotube/exfoliated graphite nanoplate composites and obtained a specific capacitance of 35 F g^{-1} at 10 mV s^{-1} in 2 M KCl electrolyte and it was higher than V_2O_5 nanotubes (25.5 F g^{-1} at 10 mV s^{-1}) [51]. Subsequently, the electrochemical performance of nanostructured SnO_2 deposited onto stainless steel electrode by potentiodynamic method was studied by Prasad et al., [52]. The capacitive behavior studied in 0.1 M Na_2SO_4 electrolyte exhibited a specific capacitance of 285 F g^{-1} at a scan rate of 10 mV s^{-1}. In addition, the synthesized porous Mn_2O_3 nanocubes exhibited a specific capacitance of 115.3 F g^{-1} at 20 mV s^{-1} in 0.5 M Na_2SO_4 with a high rate capability (58%) and a long-term cycle stability etc. [53]. Hence, the results showed that our $LiCoPO_4$ with high capacitance have great potential for use as positive electrode in supercapacitors.

3.3. Electrochemical behaviour of hybrid $LiCoPO_4$||$FeVO_4$ supercapacitor

To investigate the possibility of the prepared electrodes for practical applications, an asymmetric supercapacitor is fabricated using $LiCoPO_4$ as positive electrode and $FeVO_4$ as negative electrode. The CV curves of $LiCoPO_4$ and $FeVO_4$ in their respective potential range at 5 mV s^{-1} is shown in Fig. 6(a). $LiCoPO_4$ electrode is measured in the potential range of 0 to 0.5 V and $FeVO_4$ from 0 to −1.2 V respectively. Since the total cell voltage is the sum of the potential range of $LiCoPO_4$ and $FeVO_4$, the asymmetric supercapacitor can be operated upto 1.7 V. There is no oxygen evolution upto 1.6 V and thereafter a prominent evolution occurs. Therefore, the cyclic voltammetry and charge discharge analysis is carried out in the potential range of 0 to 1.6 V. Since, the two electrodes have different specific capacitance, there must be a perfect balance between the mass of the positive and negative electrode. The mass balancing is done based on the following equation [54],

$$\frac{m^-}{m^+} = \frac{(C^+ \times \Delta V^+)}{(C^- \times \Delta V^-)} \quad (6)$$

where m^+ and m^- are mass, C^+ and C^- are specific capacitance, ΔV^+ and ΔV^- are potential window of the positive ($LiCoPO_4$) and

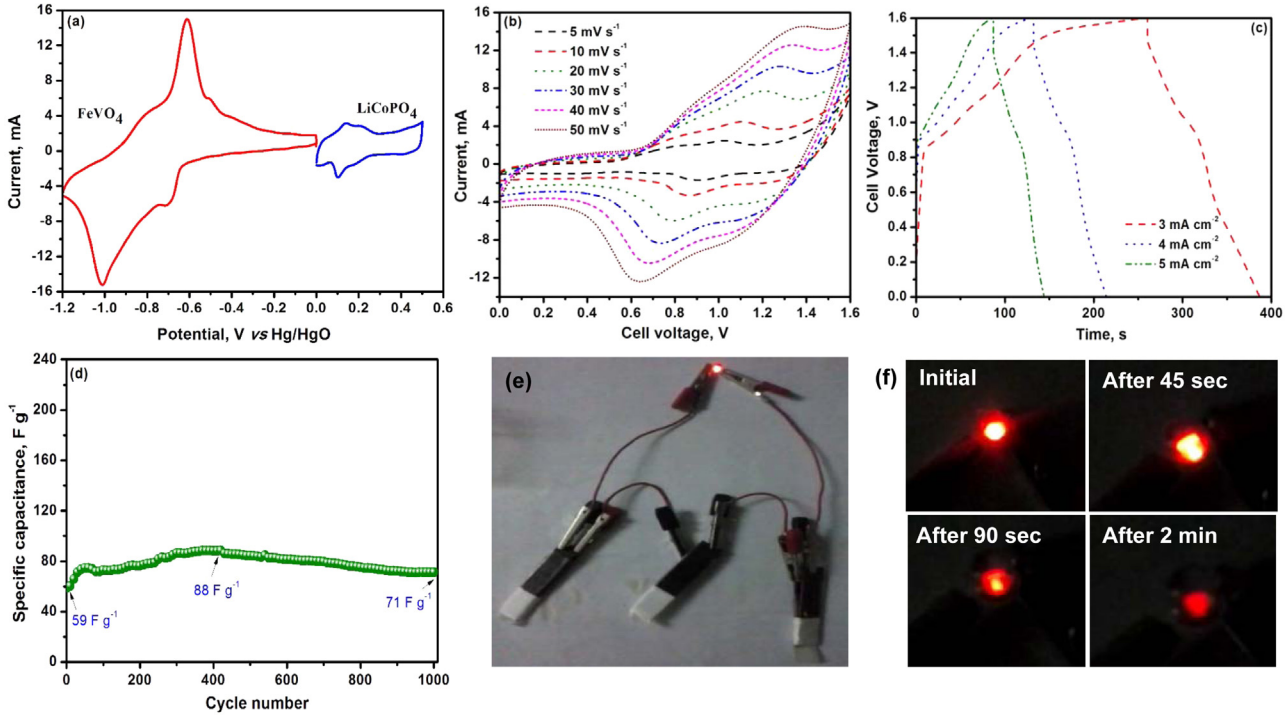

Fig. 6. (a) CV curves of $LiCoPO_4$ and $FeVO_4$ in 1 M KOH electrolyte at 5 mV/s^{-1}, (b) CV curves at various scan rates of the fabricated asymmetric supercapacitor, (c) GCD curves at various current densities, (d) Cycling stability at a current density of 5 mA/cm^{-2} of the fabricated asymmetric supercapacitor, (e) Three serially connected asymmetric supercapacitor in a charged condition and (f) Glow of a light emitting diode by the fabricated asymmetric supercapacitor at different time intervals.

negative ($FeVO_4$) electrode. After the mass being balanced, the asymmetric supercapacitor is fabricated and the performance is studied using CV and GCD analysis.

The CV curves of asymmetric supercapacitor ($LiCoPO_4$||$FeVO_4$) at various scan rates are given in Fig. 6(b). The CV curves exhibits prominent redox peaks due to the pseudocapacitive behavior of the materials. The specific capacitance values calculated for 5, 10, 20, 30, 40 and 50 mV s^{-1} are 73, 62, 52, 45, 41 and 37 F g^{-1} respectively. Fig. 6(c) shows the charge discharge curves of asymmetric $LiCoPO_4$||$FeVO_4$ at various current densities. The calculated specific capacitance is 73, 65 and 59 F g^{-1} at 3, 4 and 5 mA cm^{-2} respectively. The hybrid cell performance is usually dependent on the specific capacitance of individual electrodes. Since both the electrodes possess good specific capacitance, the hybrid supercapacitor exhibits superior performance.

The energy density and power density values for asymmetric $LiCoPO_4$||$FeVO_4$ supercapacitor is calculated using the relation,

$$E = \frac{I \int V(t)dt}{M} \quad (7)$$

$$P = \frac{E}{t} \quad (8)$$

Here, $\int V(t)\,dt$ is the integral area of the discharge curve, I is the current density, M is the mass of the active material and t is the discharge time. The calculated energy density at a current densities of 2, 3, 4 and 5 mA cm^{-2} are 27, 26, 23 and 21 Wh kg^{-1} respectively. The corresponding power densities are 484, 737, 1010 and 1326 W kg^{-1} respectively.

The cycling stability is another important requirement for practical applications of supercapacitor. The cycling stability of asymmetric $LiCoPO_4$||$FeVO_4$ supercapacitor at 5 mA cm^{-2} is given in Fig. 6(d). The initial specific capacitance of the asymmetric supercapacitor is found to be 59 F g^{-1}. There is a gradual increase in capacitance upto 400 cycles and a specific capacitance of 88 F g^{-1} is reached. This initial increase in the specific capacitance is due to the electrode activation effect [55]. Then the capacitance begins to decrease until 900 cycles thereafter it maintains a specific capacitance of 71 F g^{-1}. The corresponding energy density values is 25 Wh kg^{-1} which is higher compared with the literatures for $Ni/Ni(OH)_2$||C (21.8 Wh kg^{-1}), $Co(OH)_2$||VN (22 Wh kg^{-1}), Carbon coated $LiTi_2(PO_4)_3$||AC (14 Wh kg^{-1}), AC||MnO_2 (17.3 Wh kg^{-1}) etc [56–59].

In order to know the efficiency of the fabricated asymmetric supercapacitor, a red LED is attempted to glow. For the same, three asymmetric cells are connected serially as shown in Fig. 6(e) and it is charged upto 3.0 V. The asymmetric cells successfully powered the red light emitting diode (LED) on discharging. Fig. 6(f) shows the glowing of the LED at different time intervals. It is observed that the LED could be able to shine light for more than 2 min with considerable intensity and then only it starts to diminish. The efficiency of the fabricated asymmetric supercapacitor is found to be good and hence it could be utilized for practical applications.

4. Conclusion

$FeVO_4$ nanoparticles are successfully synthesized by simple precipitation method and were characterized using various techniques. Highly crystalline material was obtained and it was revealed through structural analysis. The particles were found to be polyhedral in their shape and sizes in the range of 100–200 nm. The d spacing values calculated from HRTEM lattice fringes confirmed the formation of $FeVO_4$. The $FeVO_4$ material exhibits a superior electrochemical performance in 1 M KOH electrolyte among the electrolyte systems studied and inferred that it might be utilized as a suitable negative electrode for pseudocapacitors. A higher specific capacitance of 972 F g^{-1} at 2 mV s^{-1} and 922 F g^{-1} at 2 mA cm^{-2} is achieved in the potential range between 0 to −1.2 V *vs.* Hg/HgO. An asymmetric hybrid supercapacitor was fabricated using $FeVO_4$ as negative and $LiCoPO_4$ as the positive electrode. The electrochemical performance of $LiCoPO_4$ as positive electrode was tested for the first time and a specific capacitance of 320 F g^{-1} was obtained at a scan rate of 5 mV s^{-1}. The asymmetric capacitor provided an excellent energy density of 21 Wh kg^{-1} at a power density of 1326 W kg^{-1} in the potential of 0 to 1.6 V.

Acknowledgement

One of the authors (V.D. Nithya) deeply thanks Department of Science and Technology (DST), New Delhi, India for providing fellowship under DST-INSPIRE program. Also, the authors would like to thank Ms. A. Rajalakshmi for her support in synthesizing $LiCoPO_4$.

References

[1] J. Zhang, X.S. Zhao, On the Configuration of Supercapacitors for Maximizing Electrochemical Performance, Chem. Sus. Chem. 5 (2012) 818–841.
[2] G. Wang, L. Zhang, J. Zhang, A review of electrode materials for electrochemical supercapacitors, Chem. Soc. Rev. 41 (2012) 797–828.
[3] B. Fang, Y.Z. Wei, K. Maruyama, M. Kumagai, High capacity supercapacitors based on modified activated carbon aerogel, J. Appl. Electrochem. 35 (2009) 229–233.
[4] A. Singh, A. Chandra, Graphite oxide/polypyrrole composite electrodes for achieving high energy density supercapacitors, J. Appl. Electrochem. 43 (2013) 773–782.
[5] G.X. Wang, J. Cai, H.F. Xu, L. Lu, H. Zhao, Enhanced capacitance of a NiO electrode prepared in the magnetic field, J. Appl. Electrochem. 44 (2014) 391–398.
[6] R. Ramya, R. Sivasubramanian, M.V. Sangaranarayanan, Conducting polymers-based electrochemical supercapacitors-Progress and prospects, Electrochim. Acta 101 (2013) 109–129.
[7] C.C. Hu, K.H. Chang, M.C. Lin, Y.T. Wu, Design and tailoring of the nanotubular arrayed architecture of hydrous RuO_2 for next generation supercapacitors, Nano Lett. 6 (2006) 2690–2695.
[8] M. Yu, J. Chen, J. Liu, S. Li, Y. Ma, J. Zhang, J. An, Mesoporous $NiCo_2O_4$ nanoneedles grown on 3D graphene–nickel foam for supercapacitor and methanol electro-oxidation, Electrochim. Acta 151 (2015) 99–108.
[9] F. Li, Y.X. Zhang, M. Huang, Y. Xing, L.L. Zhang, Rational design of porous MnO_2 tubular arrays via facile and template method for high performance supercapacitors, Electrochim. Acta 154 (2015) 329–337.
[10] L. Cui, J. Li, X.G. Zhang, Preparation and properties of Co_3O_4 nanorods as supercapacitor material, J. Appl. Electrochem. 39 (2009) 1871–1876.
[11] F. Yang, M. Zhao, Q. Sun, Y. Qiao, A novel hydrothermal synthesis and characterisation of porous Mn_3O_4 for supercapacitors with high rate capability, RSC Adv. 5 (2015) 9843–9847.
[12] Y. Li, S. Chang, X. Liu, J. Huang, J. Yin, G. Wang, D. Cao, Nanostructured CuO directly grown on copper foam and their supercapacitance performance, Electrochim. Acta 85 (2012) 393–398.
[13] D. Liu, X. Wang, X. Wang, W. Tian, J. Liu, C. Zhi, D. He, Y. Bando, D. Golberg, Ultrathin nanoporous Fe_3O_4–carbon nanosheets with enhanced supercapacitor performance, J. Mater. Chem. 1 (2013) 1952–1955.
[14] B. Sethuraman, K.K. Purushothaman, G. Muralidharan, Synthesis of mesh-like Fe_2O_3/C nanocomposite via greener route for high performance supercapacitors, RSC Adv. 4 (2014) 4631–4637.
[15] F.L. Zheng, G.R. Li, Y.N. Ou, Z.L. Wang, C.Y. Su, Y.X. Tong, Synthesis of hierarchical rippled Bi_2O_3 nanobelts for supercapacitor applications, Chem. Comm. 46 (2010) 5021–5023.
[16] D. Shu, C. Lv, F. Cheng, C. He, K. Yang, J. Nan, L. Long, Enhanced Capacitance and Rate Capability of Nanocrystalline VN as Electrode Materials for Supercapacitors, Int. J. Electrochem. Sci. 8 (2013) 1209–1225.
[17] J. Li, F. Luo, Q. Zhao, Z. Li, H. Yuan, D. Xiao, Coprecipitation fabrication and electrochemical performances of coral-like mesoporous NiO nanobars, J. Mater. Chem. A 2 (2014) 4690–4697.
[18] H. Chen, L. Hu, M. Chen, Y. Yan, L. Wu, Nickel–Cobalt Layered Double Hydroxide Nanosheets for High-performance Supercapacitor Electrode Materials, Adv. Func. Mater. 24 (2014) 934–942.
[19] M.C. Liu, L.B. Kong, L. Kang, X. Li, F.C. Walsh, M. Xing, C. Lu, X.J. Ma, Y.C. Luo, Synthesis and characterization of $M_3V_2O_8$ (M = Ni or Co) based nanostructures: a new family of high performance pseudocapacitive materials, J. Mater. Chem. A 2 (2014) 4919–4926.
[20] H. Wang, Z. Xu, H. Yi, H. Wei, Z. Guo, X. Wang, One-step preparation of single crystalline Fe2O3 particles/graphene composite hydrogels as high performance anode materials for supercapacitors, Nano Energy 7 (2014) 86–96.

[21] Y. Zhao, K. Yao, Q. Cai, Z. Shi, M. Sheng, H. Lin, M. Shao, Hydrothermal route to metastable phase $FeVO_4$ ultrathin nanosheets with exposed {0 1 0} facets: synthesis, photocatalysis and gas sensing, Cryst. Eng. Commun. 16 (2014) 270–276.
[22] K. Routray, W. Zhou, C.J. Kiely, I.E. Wachs, Catalysis Science of Methanol Oxidation over Iron Vanadate Catalysts: Nature of the Catalytic Active Sites, ACS Catal. 1 (2011) 54–56.
[23] D.H. Sim, X. Rui, J. Chen, H. Tan, T.M. Lim, R. Yazami, H.H. Hng, Q. Yan, Direct growth of $FeVO_4$ nanosheet arrays on stainless steel foil as high-performance binder-free Li ion battery anode, RSC Adv. 2 (2012) 3630–3633.
[24] V.D. Nithya, R. Kalai Selvan, Synthesis, electrical and dielectric properties of $FeVO_4$ nanoparticles, Physica B 406 (2011) 24–29.
[25] V.D. Nithya, R. Kalai Selvan, C. Sanjeeviraja, D. Mohan Radheep, S. Arumugam, Synthesis and characterization of $FeVO_4$ nanoparticles, Mater. Res. Bull. 46 (2011) 1654–1658.
[26] Q.T. Qu, B. Wang, L.C. Yang, Y. Shi, S. Tian, Y.P. Wu, Study on electrochemical performance of activated carbon in aqueous Li_2SO_4, Na_2SO_4 and K_2SO_4 electrolytes, Electrochem. Comm. 10 (2008) 1652–1655.
[27] R. Wang, Q. Li, L. Cheng, H. Li, B. Wang, X.S. Zhao, P. Guo, Electrochemical properties of manganese ferrite-based supercapacitors in aqueous electrolyte: The effect of ionic radius, Colloids and Surfaces A: Physicochem. Eng. Aspects 457 (2014) 94–99.
[28] A. Rajalakshmi, V.D. Nithya, K. Karthikeyan, C. Sanjeeviraja, Y.S. Lee, R. Kalai Selvan, Physicochemical properties of V^5 + doped $LiCoPO_4$ as cathode materials for Li-ion batteries, J. Sol–Gel Sci. Technol. 65 (2013) 399–410.
[29] S.M. Pourmortazavi, M.R. Nasrabadi, M.K. Shalamzari, M.M. Zahedi, S.S. Hajimirsadeghi, I. Omrani, Synthesis, structure characterization and catalytic activity of nickel tungstate nanoparticles, Appl. Surf. Science 263 (2012) 745–752.
[30] V. Manivannan, J.B. Goodenough, Low-temperature synthesis of rutile VO_2 in aqueous solution using $NH_2OH{\cdot}HCl$ as reducing agent, Mater. Res. Bull. 33 (1998) 1353–1357.
[31] Z. Wang, Y. Zuo, Y. Yao, L. Xi, J. Du, J. Wang, D. Xue, Microwave absorption properties of amorphous iron nanostructures fabricated by a high-yield method, J. Phys. D: Appl. Phys. 46 (2013) 135002–135008.
[32] D.M. Fernandes, R. Silva, A.A. Winkler Hechenleitner, E. Radovanovic, M.A. Custodio Melo, E.A. Gomez Pineda, Synthesis and characterization of ZnO, CuO and a mixed Zn and Cu oxide, Mater. Chem. Phys. 115 (2009) 110–115.
[33] Q. An, J. Sheng, X. Xu, Q. Wei, Y. Zhu, C. Han, C. Niua, L. Mai, Ultralong $H_2V_3O_8$ nanowire bundles as a promising cathode for lithium batteries, New J. Chem. 38 (2014) 2075–2080.
[34] F.J. Quites, H.O. Pastore, Hydrothermal synthesis of nanocrystalline VO_2 from poly (diallyldimethylammonium) chloride and V_2O_5, Mater. Res. Bull. 45 (2010) 892–896.
[35] A.S. Vuk, B. Orel, UV–Visible and IR spectroelectrochemical studies of $FeVO_4$ sol–gel films for electrochromic applications, J Sol–Gel Sci. Tech. 23 (2002) 165–181.
[36] P. Tabero, Synthesis and properties of $Fe_{0.83}V_{1.17}O_4$, J. Therm. Anal. Calorim. 113 (2013) 247–252.
[37] A.S. Vuk, B. Orel, G. Drazic, IR spectroelectrochemical studies of $Fe_2V_4O_{13}$, $FeVO_4$ and $InVO_4$ thin films obtained via sol–gel synthesis, J. Solid State Electrochem. 5 (2001) 437–449.
[38] M. Alagiri, S. Ponnusamy, C. Muthamizhchelvan, Synthesis characterization of NiO nanoparticles by Sol–gel Method, J. Mater Sci: Materials in Electronics 23 (2012) 728–732.
[39] Q. Qu, S. Yang, X. Feng, 2D Sandwich-like sheets of iron oxide grown on graphene as high energy anode material for supercapacitors, Adv. Mater. 23 (2011) 5574–5580.
[40] Q. Qu, P. Zhang, B. Wang, Y. Chen, S. Tian, Y. Wu, R. Holze, Electrochemical performance of MnO_2 nanorods in neutral aqueous electrolytes as a cathode for asymmetric supercapacitors, J. Phys. Chem. C 113 (2009) 14020–14027.
[41] R.N. Reddy, R.G. Reddy, Sol–gel MnO_2 as an electrode material for electrochemical capacitors, J. Power Sources 124 (2003) 330–337.
[42] N. Nagarajan, I. Zhitomirsky, Cathodic electrosynthesis of iron oxide films for electrochemical supercapacitors, J. Appl. Electrochem. 36 (2006) 1399–1405.
[43] L.M. Chen, Q.Y. Lai, H.M. Zeng, Y.J. Hao, J.H. Huang, Effects of various factors on capacitive properties of $VO_x{\cdot}nH_2O$ powders in aqueous electrolyte, J. Appl. Electrochem. 41 (2011) 299–305.
[44] V.D. Nithya, R. Kalai Selvan, L. Vasylechko, C. Sanjeeviraja, Surfactant assisted sonochemical synthesis of Bi_2WO_6 nanoparticles and their improved electrochemical properties for use in pseudocapacitors, RSC Adv. 4 (2014) 4343–4352.
[45] X.J. Zhu, H.L. Dai, J. Hu, L. Ding, L. Jiang, Reduced graphene oxide–nickel oxide composite as high performance electrode materials for supercapacitors, J. Power Sources 203 (2012) 243–249.
[46] D. Han, P. Xu, X. Jing, J. Wang, D. Song, J. Liu, M. Zhang, Facile approach to prepare hollow core–shell NiO microspherers for supercapacitor electrodes, J. Solid State Chem. 203 (2013) 60–67.
[47] Q. Wang, Z. Wen, J. Li, A hybrid supercapacitor fabricated with a carbon nanotube cathode and a TiO_2-B nanowire anode, Adv. Funct. Mater. 16 (2006) 2141–2146.
[48] K. Krishnamoorthy, G.K. Veerasubramani, S. Radhakrishnan, S.J. Kim, Structuring materials for lithium-ion batteries: Advancements in nanomaterial structure, composition, and defined assembly on cell performance, Chem. Eng. J. 251 (2014) 116–122.
[49] J. Tang, D. Liu, Y. Zheng, X. Li, X. Wang, D. He, Effect of Zn-substitution on cycling performance of α-$Co(OH)_2$ nanosheet electrode for supercapacitors, J. Mater. Chem. A 2 (2014) 2585–2591.
[50] P. Justin, G. Ranga Rao, CoS spheres for high rate electrochemical capacitive energy storage applications, Int. J. Hydrogen Energy 35 (2010) 9709–9715.
[51] J.S. Bonso, A. Rahy, S.D. Perera, N. Nour, O. Seitz, Y.J. Chabal, K.J. Balkus Jr., J.P. Ferraris, D.J. Yanga, Exfoliated graphite nanoplatelets–V_2O_5 nanotube composite electrodes for Supercapacitors, J. Power Sources 203 (2012) 227–232.
[52] K.R. Prasad, N. Miura, Electrochemical synthesis and characterization of nanostructured tin oxide for electrochemical redox supercapacitors, Electrochem. Comm. 6 (2004) 849–852.
[53] W. Li, J. Shao, Q. Liu, X. Liu, X. Zhou, J. Hu, Facile synthesis of porous Mn_2O_3 nanocubics for high rate supercapacitors, Electrochim. Acta 157 (2015) 108–114.
[54] J. Yan, Z. Fan, W. Sun, G. Ning, T. Wei, Q. Zhang, R. Zhang, L. Zhi, F. Wei, Advanced asymmetric supercapacitors based on $Ni(OH)_2$/Graphene and porous graphene electrodes with high energy density, Adv. Funct. Mater. 22 (2012) 2632–2641.
[55] L. An, K. Xu, W. Li, Q. Li, B. Li, R. Zou, Z. Chen, J. Hu, Exceptional pseudocapacitive properties of hierarchical NiO ultrafine nanowires grown on mesoporous NiO nanosheets, J. Mater. Chem. A 2 (2014) 12799–12804.
[56] Y.Z. Su, K. Xiao, N. Li, Z.Q. Liu, S.Z. Qiao, Amorphous $Ni(OH)_2$ @ three-dimensional Ni core–shell nanostructures for high capacitance pseudocapacitors and asymmetric supercapacitors, J. Mater. Chem. A 2 (2014) 13845–13853.
[57] R. Wang, X. Yan, J. Lang, Z. Zheng, P. Zhang, A hybrid supercapacitor based on flower-like $Co(OH)_2$ and urchin-like VN electrode materials, J. Mater. Chem. A 2 (2014) 12724–12732.
[58] V. Aravindan, W. Chuiling, M.V. Reddy, G.V. Subba Rao, B.V.R. Chowdari, S. Madhavi, Carbon coated nano-$LiTi_2(PO_4)_3$ electrodes for non-aqueous hybrid supercapacitors, Phys. Chem. Chem. Phys. 14 (2012) 5808–5814.
[59] T. Cottineau, M. Toupin, T. Delahaye, T. Brousse, D. Belanger, Nanostructured transition metal oxides for aqueous hybrid electrochemical supercapacitors, Appl. Phys. A: Mater. Sci. Process 82 (2006) 599–606.